# Materials selection for optimum energy production by double layer expansion methods

*Guillermo R. Iglesias*[a], *María M. Fernández*[a], *Silvia Ahualli*[a], *María L. Jiménez*[a], *Oleksander P. Kozynchenko*[b], *Ángel V. Delgado*[a,*]

[a]Department of Applied Physics, School of Sciences, University of Granada, 18071 Granada, Spain

[b]MAST Carbon Ltd., Henley Park, Guildford, Surrey GU3 2AF, UK

[*] **Corresponding Author.**

Departament of Applied Physics, School of Sciences, Campus Fuentenueva. University of Granada, 18071 Granada, Spain.

E-mail: adelgado@ugr.es. (Ángel V. Delgado)

**Author Contributions.** The manuscript was written through contributions of all authors. All authors have given approval to the final version of the manuscript. All authors contributed equally.

ABSTRACT

The capacitive mixing procedure for energy extraction based on Double Layer Expansion (CDLE) belongs to the group of so-called CAPMIX techniques, which aim at obtaining energy from the salinity difference between fresh and sea waters. Specifically, the CDLE technique takes advantage of the voltage rise that occurs when sea water is exchanged for river water in a pair of porous electrodes which jointly behave as an electrical double layer supercapacitor. In this article, we deal with some experimental aspects that appear essential for optimizing the extracted energy, and have not yet been analyzed with sufficient detail. This investigation will help in evaluating those parameters which need to be fixed in a future CDLE device. These include the charging potential, the durations of the different cycle steps, the load resistance used, and the porosity and hydrophilicity of the carbon.

**Keywords:** Activated carbon particles; capacitive energy extraction; double layer expansion; pore size distribution; supercapacitors; wettability.

# 1. Introduction

It is hard to find fields of science and technology where advances are of larger significance for the future of our planet than in the area of clean energy production. Interestingly, the physical chemistry of interfaces has found a niche in this area, as it did previously in decontamination of soils and water, as shown in [1, 2], for example. This new field refers to the possibility of net energy extraction based on the electrical potential rise in an electrical double layer when the ionic strength is reduced at constant charge: the associated technique has been called *CDLE* or *Capacitive energy extraction based on Double Layer Expansion*. It is one of the so-called *CAPMIX* techniques [3], in which energy is intended to be extracted taking advantage of the electrochemistry of the porous electrode-solution interface, as in the rapidly advancing technology of supercapacitors or electric double layer (EDL) capacitors [4, 5].

A related technique is known as *CDP*, for *Capacitive energy extraction based on Donnan Potential*. In this, a pair of electrodes is charged by means, respectively, of cation- and anion-exchange membranes in contact with each of them. As in CDLE, solution exchange is also required, and current flows through the external circuit in alternate directions when sea water is exchanged for fresh water and vice versa [6-9]. These technologies add to other, more classical ones, such as pressure-retarded osmosis (PRO) [10, 11] and reverse electrodyalisis (RED) [12, 13], reciprocal of well-known desalination techniques. Although some of them have reached the plant production scale [14], they are mostly at the laboratory or prototype plant stage.

The technique that we are interested in is CDLE, firstly conceived by Brogioli [15], and implemented experimentally by Brogioli et al. [16]. Models on the phenomenon and its kinetics

have been developed by Rica et al. [17–19], and Jiménez et al. [20]. A pair of electrodes are connected to an external power source while wetted with a salt solution of high concentration (sea water); then, the solution is exchanged for a low-concentration one (fresh or river water) in open circuit (constant charge). The subsequent EDL expansion gives rise to an increase of the potential, and finally the charge is transferred back to the external source. Since this transfer occurs at a higher potential, more energy is recovered than was initially given to the system. Hence, the key points are the use of microporous carbon electrodes providing a very high surface area (up to 2000 $m^2/g$) and a suitable procedure for charging/discharging them. Fig. 1 is a schematic view of the CDLE cycle:

- **Step 1**. Electrodes immersed in salty water are connected to a battery set at a certain potential $V_0$. Ions redistribute in the solution until a certain electronic charge grows at the electrode surface and the potential reaches the battery potential. That is point A in Fig. 1.
- **Step 2**. The battery is disconnected and salty water is replaced by fresh water giving rise to double layer expansion. The surface potential increases because the capacitance decreases at a constant surface charge. Point B.
- **Step 3**. The battery is reconnected to the electrode, which is now at a higher potential. Hence, a current flows back to the battery as a consequence of this potential difference. Point C.
- **Step 4**. The battery is disconnected and the fresh water is replaced by salty water again, leading to a further decrease of the voltage below the battery value. Point D.

The net work, $W_2$ - $W_1$, is the shadowed area in the Figure, which is roughly proportional to the product of the voltage rise in step 2 and the charge exchanged in step 3.

A great variety of activated carbons can be tailored to serve as active material. The system can be implemented in such a way that repeated automatic cycling is performed until a steady behavior is obtained, but in spite of the apparent simplicity of the EDL universal properties, the predictability of the results is limited. This is because the measured quantities (in brief, potential difference between the electrodes in the cell and current from one to the other as a function of time) are a macroscopic average of values which can change from one position to another in the electrode in distances smaller than the electrode thickness [21]. In fact, although the walls of the pores can be considered equipotential in open circuit throughout the whole electrode, the surface charge may behave differently, considering that a concentration profile will be established along the electrode, and that the EDLs can be quite different in macro- and micropores [17–20, 22–24].

The main topic of the present contribution is the evaluation of the experimental parameters determining the optimization of the CDLE cycle performance. It can be expected that the carbon characteristics, in particular, hydrophilicity of the carbon pore walls and pore structure, will be determinant. In fact, it is well known that the electrochemical response of EDL supercapacitors is strongly dependent on the degree of fitting of the pore and solvated ion sizes [25]. Important effects have also been reported of the size and diffusion coefficient of the ions in solution. Because of the expected use of natural water sources in the Capmix techniques we are forced to use $Na^+$ as cation, but this is not a drawback, since both $K^+$ and $Na^+$ have been found most suitable in aqueous electrolytes for supercapacitor applications [25]. Additionally, the implementation of the cycle will also make a significant contribution: the power production will be first of all affected by the kinetics of the process. Hence, it will be necessary to investigate the time settings for the different cycle stages. However, this will also affect the useful power transfer to the external load, the resistance of which must be properly chosen as well. Finally,

although one could think that the potential rise is an intrinsic property of the EDL, the effect of the potential difference applied during the charging step might also affect the whole process even if the voltage is kept below the minimum value for faradaic reactions. In fact, such an effect was observed in the earliest implementations of the methods [16].

# 2. Experimental

## 2.1 Materials

MAST Carbon International (UK) provided 6 different carbon samples for this study. All of them were characterized by nitrogen adsorption isotherms, from which pore size distributions were calculated using the Barrett-Joyner-Halenda (BJH) model [26]. Carbon preparation details are provided as Supporting Information, and they can also be found in [27, 28]. Fig. 2 is a TEM image of one of the samples used (TE11), where the presence of the internal porosity is evident.

Sodium chloride was from Sigma Adrich (USA), and water used in the preparation of the solutions was deionized and filtered in a Milli-Q Academic system from Millipore (USA). External connections were perforated platinum disks, 9 mm in radius.

## 2.2 Methods

The wettability of the carbon samples was characterized via contact angle determinations at room temperature (20 ± 1 $^{o}$C) using a Ramé-Hart 100-00 230 goniometer (USA) provided with a Pixelink PL-A662 CCD camera (Canada). The electrophoretic mobility was measured with a Malvern Nano ZS (Malvern Instruments, UK). For the salinity exchange experiments, ~0.3 g of carbon particles (or a disk of the cast carbon layer) were packed on the electrode and maintained

in place by means of a cellulose membrane and a plastic or stainless steel ring. Fig. 3 includes a picture of one electrode and of the final electrode configuration.

The pair of electrodes was placed in parallel configuration at the specified distance, which was measured with calipers. A glass cylindrical cell with vertical inlet and outlet tubes was used as shown in Fig. 3b. Salt and fresh water reservoirs were placed some 50 cm above the electrode level, and three electrovalves (VDW31-4G-2, 2/3 Port Solenoid Valve, SMC Company, USA) were employed for filling and emptying the cell through the bottom tube. A Keithley 2700 (USA) multimeter provided with a data acquisition card was used to measure the potential difference between the electrodes, and the current going in or out of the cell, and these data were stored at specified time intervals (typically, 5 s). The charging source was a supercapacitor (Bootscap cell supercapacitor, C = 350 F, Maxwell Technologies, USA), which was also used in the discharging stage, through a selected load resistor. A PIC microcontroller (PIC16F684, Microchip Technology Inc., USA) was used for performing the different stages of the process at specified intervals.

# 3. Results and Discussion

## 3.1 Overall cycle shape

In Fig. 4 we can observe all the stages of the CDLE cycle. Note that after charging (step 1), a transition region is produced due to the emptying of the cell and the exchange of sea and fresh water solutions. The slowest stage of the cycle is the voltage rise in open circuit (step 2). In the discharging step (step 3) the cell voltage undergoes a rapid decay (BB’) followed by a progressive discharge. The reason of this decay is the non-zero value of the internal resistance,

specially in fresh water. This can be controlled to some extent by proper selection of the load resistance as it will be discussed below. Still another transition region follows before step 4, when the cell is connected again to the external supercapacitor. The kinetics of step 2 is controlled by ion diffusion processes inside the EDLs of the pores. The same can be said about the step 4. On the contrary, steps 1 and 3 can be easily modelled by simulating the porous carbon plug as a capacitor with an internal resistance. The two main quantities directly related to the extracted energy will be the transferred charge in the B'C step and the potential difference AB'. Hence, maximizing their product will lead to the optimum extracted energy.

Fig. 5 is an illustration of the simple modelling that can be implemented to get some insight of the basis of the charging and discharging processes. The circuit proposed is a simplification of the more detailed model of the pores as transmission lines with distributed resistances and capacitances, as described in [23, 24, 29]. However, for our purposes the description based on the whole transmission line requires long computational times without significant accuracy increase as compared to the simplified network in Fig. 5.

In such schematic network, the capacitor $C$ represents the EDL capacitor contribution on both electrodes. The internal resistance $R_{int}$ will be interpreted as a sum of the contribution of the wall resistance to electron flow, the resistance of the solution permeating the pores where only ionic currents are possible, and the resistance associated to the solution between the two electrodes.

As shown in Fig. SI-1 (Supplementary Information), it is possible to accurately model the charge and discharge processes using reasonable values of the quantities involved. Both in the experimental data and the modelling it can be observed that there are two well-separated time scales so that both the current through the cell and the overall potential present an initial rapid change followed by a much slower response. The extent of such decay will depend on $R_{discharge}$, $R_{int}$, and $C$.

The selection of $R_{discharge}$ will determine, together with $R_{int}$, the current at which the cell discharges through the external device, and hence the charge transferred in step 3 of Fig. 4: the charge will be larger the smaller $R_{discharge}+R_{int}$. In addition, the *useful* potential jump depends on the two resistances in opposite ways, increasing with the latter and decreasing with the former. A well-known result is that the maximum rate of power transfer to the external device will occur when $R_{discharge}=R_{int}$. In our device, for a given carbon configuration, the internal resistance will depend on the separation between the electrodes (which also determines the existence of sufficient solution volumes for exchanging), so that closer separations will provide larger energy per cycle, as experimentally demonstrated by the data in Fig. SI-2a. Once the minimum value is found for $R_{int}$, the energy obtained (for given values of the remaining experimental parameters, as discussed below) will be maximum when the mentioned equality between resistances is fulfilled. Fig. SI-2b illustrates this with an example.

## 3.2 Charging potential effects

Because of the need of avoiding chemical reactions, the potential applied to the electrodes should never be higher than approximately 1 V [4], but below that value we have a whole range of charging potentials, and their effect on the CDLE performance must be considered. This is illustrated in Fig. 6, where CDLE cycles are plotted for TE11 carbon powder in the form of potential vs. time (a), together with the voltage rise (b) and the transferred charge in step 3 (c) with Norit films, for different charging potentials. This Figure demonstrates that:

- The voltage rise when fresh water is exchanged by salt water is symmetric with respect to the drop in the reverse exchange only at intermediate potentials. At low charging

voltages, the former is smaller in amplitude, whereas for high potentials, the situation is the opposite.

- The rise at both high and low potentials is lower than at intermediate ones.
- The amount of charge exchanged undergoes a similar dependence on charging potential.

The results offer a clue as to the optimum working conditions in the CDLE technique, but their justification is by no means straightforward. At very low voltages, calculations of the charge-potential in a swarm of spherical particles considering ion size [20] indicate that the potential drop in salt water is smaller than its rise in fresh water, if double layers are equilibrated with the corresponding solutions. At larger potential, the model predicts identical voltage differences, as in fact observed experimentally; this is the optimal working range. If, however, the potential used for charging is raised even more, a new effect (not considered in equilibrium models) is evidenced, and that is the self-discharge of the electrodes, because of current leakage, higher the larger the applied voltage [16]. Such leakage has been ascribed to the tendency of the electrodes to attain their equilibrium surface potential, generated, as many other sources of surface charge, by adsorption of species from solution or dissociation of surface groups [30]. The presence of redox reactions in the carbon-solution interface is likely as well. The actual reason, however, is not completely clear, although it has been found in all kinds of EDL-based supercapacitors [23, 24]. In addition, the difficulty for complete exchange of salty water by fresh one will always be present, contributing to increasing the salinity of the pores above the nominal equilibrium value, this in turn leading to a lower potential rise. Overall, this goes against the charge transfer in the CDLE cycle and hence against energy production [20].

## 3.3 Switching time settings

The potential rise in the CDLE cycle is not instantaneous, since it is necessary that ions migrate out of pore spaces when fresh water get in the electrode. There are two factors that act against each other in optimizing power extraction: it would appear best to wait until the potential does not grow beyond its maximum but at the same time waiting too long would mean smaller power for a given charge transferred. Even worse, the voltage in the CDLE cell might decrease as mentioned due to leakage, this producing lower extracted energy and further decrease in the power. The results presented in Fig. SI-3 confirm these ideas. Note that after 3 min rising time the energy goes through a maximum (Fig. SI-3a) even though the potential remains constant after that time (Fig. SI-3b). In the example shown, switching from step 2 to step 3 should be carried out in no more than 3 minutes even though the potential might keep rising for longer time, as leakage will become increasingly important and, as a consequence, power production will be compromised.

## 3.4 The role of carbon wettability

This is obviously a determinant property of the electrodes. In the Capmix techniques, the need for exchange brings about the requirement that ions in the EDLs should be able to go in and out of them and they will most probably be hydrated, at least partially. The hydrophilicity of the carbon used for the electrode preparation is hence an important issue.

In order to check for this, we prepared two kinds of carbon particles, named SC-1 and SC-2 hereafter, with almost identical pore size distribution, but quite different in their hydrophobic/hydrophilic balance. Fig. 7 shows the great similarity between both samples,

concerning their pore sizes. With this, we can be sure that the differences in CDLE performance, if any, must come from their different surface characteristics.

With the aim of characterizing the wettability properties of these samples, we carried out contact angle measurements, as explained in the section **Surface free energy determinations** of the Supporting Information. Basically, the surface free energy of the solids (a mesaure of their wettability: a high-surface energy solid will be more hydrophilic) is obtained from the contact angle hysteresis (difference between advancing and receding contact angles), as described in [31, 32]. One example is presented in Fig. SI-4, where the differences between samples SC-1 and SC-2 is evident.

The results are presented in Table 1, together with the surface free energy calculated by means of Eq. (SI-1). The Table also contains the data pertaining to the samples SR which will be used for our analysis of the effect of pore size distribution (see below).

It is easy to conclude that sample SC-1 is very hydrophobic whereas carbon SC-2 is, on the contrary, characterized by hydrophilic behavior. This is demonstrated by the data shown in Table 1, where we find low surface free energy and large contact angles for SC-1 and the opposite situation for sample SC-2.

An independent characterization of the hydrophobicity can be done by electrophoretic determinations of the samples as a function of pH. This quantity is extremely sensitive to the electric state of the particle surface. In the section **Electrophoretic mobility of SC-1 and SC-2** of the Supporting Information the differences between the surfaces of SC-1 and SC-2 particles is corroborated.

We can now explain the results obtained when the two carbons are used in CDLE cycles, shown in Fig. 8: the fact that hydrophobicity hinders the required ion exchange is evident. The voltage rise in SC-1 is almost negligible for otherwise identical conditions. In fact, the results in Table 2 quantitatively demonstrate the important differences between the carbon samples regarding their CDLE performance.

### 3.5 Samples with different pore size distributions

It can be foreseen that pore size distribution must also be an essential property of the carbon used in the CDLE process, for some reasons. One is the possibility of EDL overlap in the pores (and eventually constant potential inside them), which is clearly dependent on the channel dimensions. Secondly, the ratio between the ion and pore sizes determines the ease with which the ions can diffuse inside, and even if they are hydrated or (at least, partially) dehydrated [25]. In addition, the amount of charge transferred is limited by the possibility of EDL saturation (even pore saturation in the case of small pore radius) due to the finite volume of counterions. All these aspects might be determinant in the resulting kinetics (associated to the rate of ion adsorption-desorption in the EDL) and energy production (as the voltage rise and charge transferred will be reduced if ion exchange is incomplete). Even if exchange is not required, as in the supercapacitor technology [25, 33], the pore size distribution is considered as the most important design parameter, taking into account the relationship between microstructure and ion accessibility to the pores.

In order to analyze the implications of the pore size distribution on CDLE, we used the samples SR-03, SR-23 and SR-51, with different pore structures, as shown in Fig. 9. The three samples can be however considered as equivalent from the point of view of their surface free

energy. The data displayed in Table 1 indicate that they are moderately hydrophobic (with surface free energies closer to that of SC-1 than to SC-2). Fig. SI-5 gives us further indication of the similarities of the surfaces from the electrochemical point of view: the electrophoretic mobility $u_e$ of the three kinds of carbon particles is plotted as a function of pH in 1 mM NaCl. Note that the mobilities measured are intermediate between those of SC-1 and SC-2 (Fig. SI-6), confirming that the treatment applied for the pore size variation does not affect the electrical surface functionalities sufficiently as to alter the wettability of the carbons.

The important point here is the consideration of the effects of the pore size distribution on the CDLE response. Table 3 shows some preliminary results, obtained with layers of the indicated carbon particles. Although the theoretical predictions [20] indicate that the effect of the average pore size on the voltage rise should be negligible, our data show that this is true for samples SR-03 and SR-51 whereas SR-23 deviates from this constancy and produces a slightly lower voltage increase. Considering that SR-51 contains a significant amount of pores in the 5-10 nm range, our results can be explained by assuming that the larger pore fraction behaves as a sort of solution reservoir, in which salt and fresh solutions are easily exchanged, leading to a favorable diffusion of counterions in and out of the small pores. It appears as if the proportion of mesopores in SR-23 were not enough to compensate for its largely reduced surface area, in comparison with SR-03. Interestingly enough, the "useful" voltage rise, $V_{AB'}$, is similar for the three samples, an indication of their internal resistance being different. As a result, it is the transferred charge that dominates the energy production: the small pore size of SR-03 becomes here the controlling parameter, leading to a value of charge almost double in this sample than in the other two. This finally explains the great advantage of using carbons with all their pores in the 1 nm size range, as the energy obtained per cycle is clearly maximum in this case (64 μJ in SR-03, to be compared to 18μJ in SR-23 and 27μJ in SR-51). Such a maximum is associated to

the amount of transferred charge, and this is the true advantage of using the smallest pore size, and not so the voltage rise, very similar in all cases.

In addition, there is a very noticeable difference between the three samples: the rate of elevation of the voltage when the solutions are exchanged is much faster for SR-03 (i.e., the sample with smallest average pore size) than for the others (Fig. 10). The diffusion distance of ions must be shorter in that sample, allowing for a faster redistribution of the surface charge than in carbons containing larger pores. Furthermore, counterions can lose their hydration layers when entering the narrow channels, leading to larger diffusion coefficient and easier migration in the channels [34, 35]. It is remarkable that such different rates allow us to predict a larger power (not only energy) in carbon SR-03.

## 4. Conclusions

Summarizing, energy production based on electric double layer expansion can be significantly improved if electrode materials are properly selected. In particular, if activated carbon particles are used, it is best to use hydrophilized material: this might look counter-intuitive, since carbon oxidation can be favored in such case. However, the fact that hydrated ions must be cyclically exchanged with the contacting solutions compensate for this possible drawback. The average pore size, in relation with the EDL thickness and the ion diameter is, as expected another determinant quantity. Optimum CDLE results will be obtained if the carbon used in the electrodes has a predominant pore population in the 1 nm region.

**Supporting Information**. In the supporting information accompanying this manuscript information is provided on: i) carbon preparation and experimental cell details; ii) circuit

modeling and effects of experimental parameter selection on the CDLE performance; iii) surface free energy determinations; iv) electrophoretic mobility of samples SC-1 and SC-2; v) characteristics of SR samples; This material is available free of charge via the Internet at http://www.sciencedirect.com.

**Acknowledgement**

The research leading to these results received funding from the European Union 7th Framework Programme (FP7/2007-2013) under agreement No. 256868. Further financial support from Junta de Andalucía (Spain), project PE-2008-FQM3993 is also gratefully acknowledged.

**REFERENCES**

[1] M. Hamerski, J. Grzechulska, A. Morawski, Solar Energy 66 (1999) 395 – 399.

[2] B. Schrick, B. W. Hydutsky, J. L. Blough, T. E. Mallouk, Chem. Mater. 16 (2004) 2187–2193.

[3] M. Bijmans, O. Burheim, M. Bryjak, A. Delgado, P. Hack, F. Mantegazza, S. Tenisson, H. Hamelers, Energy Procedia 20 (2012) 108 – 115.

[4] B. Conway, Electrochemical Supercapacitors: Scientific Fundamentals and Technological Applications, Kluwer Academic, New York, 1999.

[5] P. Sharma, T. Bhatti, Energy Conversion and Management 51 (2010) 2901 – 2912.

[6] B. B. Sales, M. Saakes, J. W. Post, C. J. N. Buisman, P. M. Biesheuvel, H. V. M. Hamelers, Environ. Sci. Technol. 44 (2010) 5661–5665.

[7] B. B. Sales, F. Liu, O. Schaetzle, C. J. Buisman, H. V. M. Hamelers, Electrochimica Acta 86 (2012) 298 – 304.

[8] O. S. Burheim, F. Liu, B. B. Sales, O. Schaetzle, C. J. N. Buisman, H. V. M. Hamelers, J. Phys. Chem. C 116 (2012) 19203–19210.

[9] F. Liu, O. Schaetzle, B. B. Sales, M. Saakes, C. J. N. Buisman, H. V. M. Hamelers, H. V. M. Environ. Sci. Technol. 5 (2012) 8642–8650.

[10] A. Seppala, M. J. Lampinen, J. Membr. Sci. 161 (1999) 115–138.

[11] S. Chou, R. Wang, L. Shi, Q. She, C. Tang, A. Fane, J. Membr. Sci. 389 (2012) 25 – 33.

[12] J. N. Weinstein, F. B. Leitz, Science 191 (1976) 557–559.

[13] S. Mulyati, R. Takagi, A. Fujii, Y. Ohmukai, T. Maruyama, H. Matsuyama, J. Membr. Sci. 417-418 (2012) 137–143.

[14] J. Veerman, M. Saakes, S. J. Metz, G. J. Harmsen, Chem. Eng. J. 166 (2011) 256–268.

[15] D. Brogioli, Phys.Rev. Lett. 103 (2009) 058501.

[16] D. Brogioli, R. Zhao, P. M. Biesheuvel, Energy Environ. Sci. 4 (2011) 772–777.

[17] R. A. Rica, D. Brogioli, R. Ziano, D. Salerno, F. Mantegazza, J.Phys. Chem. C 116 (2012) 16934–16938.

[18] R. A. Rica, R. Ziano, D. Salerno, F. Mantegazza, D. Brogioli, Phys.Rev. Lett. 109 (2012) 156103.

[19] R. A. Rica, R. Ziano, D. Salerno, F. Mantegazza, M. Z. Bazant, D. Brogioli, Electrochimica Acta 92 (2013) 304 – 314.

[20] M. L. Jiménez, M. M. Fernández, S. Ahualli, G. Iglesias, A. V. Delgado, J. Colloid Interface Sci. 402 (2013) 340 – 349.

[21] J. S. Newman, C. W. Tobias, J. Electrochem. Soc. 109 (1962), 1183–1191.

[22] M. Z. Bazant, M. S. Kilic, B. D. Storey, A. Ajdari, A. Adv. Colloid Interface Sci.152 (2009) 48–88.

[23] M. Kaus, J. Kowal, D. U. Sauer, Electrochimica Acta 55 (2010) 7516-7523.

[24] J. Kowal, E. Avaroglu, F. Chamekh, A. Šenfelds, T. Thien, D. Wijaya, D. U. Sauer, J. Power Sources 196 (2011) 573–579.

[25] Q. T. Qu, B. Wang, L. C. Yang, Y. Shi, S. Tian, Y. P. Wu, Electrochem. Commun. 10 (2008) 1652-1655.

[26] E. P. Barrett, L.G. Joyner, P. P. Halenda, J. American Chem. Soc.73 (1951) 373–380.

[27] S. Tennison, O. Kozynchenko, V. Strelko, A. Blackburn, A. US Pat. US20040024074 A1, 2004.

[28] J. L. Figueiredo, M. F. R. Pereira, M. M. A. Freitas, J. J. M. Orfao, Carbon 37 (1999) 1379–1389.

[29] M. Bazant, Spring 2011. (Massachusetts Institute of Technology: MIT OpenCourseWare, http://ocw.mit.edu (Accessed 13 Mar, 2013). License: Creative Commons BY-NC-SA.

[30] D. Brogioli, R. Ziano, R. A. Rica, D. Salerno, O. Kozynchenko, H. V. M. Hamelers, F. Mantegazza, Energy Environ. Sci. 5 (2012) 9870–9880.

[31] E. Chibowski, Adv. Colloid Interface Sci. 133 (2007) 51–59.

[32] E. Chibowski, 2ndInternational Symposium on Contact Angle, Wettability and Adhesion, Newark, NJ, Jun 21-23, 2000.

[33] M. Endo, T. Takeda, Y. J. Kim, K. Koshiba, K. Ishii, K. Carbon Science 1 (2001) 117–128.

[34] J. Chmiola, C. Largeot, P. L. Taberna, P. Simon, Y. Gogotsi, Angew. Chem. International Edition 47 (2008) 3392–3395.

[35] A. Tanimura, A. Kovalenko, F. Hirata, Chem. Phys. Lett. 378 (2003) 638 – 646.

**List of TABLES**

**Table 1**. Advancing and receding contact angles of water on samples SC-1, SC-2, SR03, SR-23 and SR-51. The receding angle in SC-2 was not significantly distinct from zero. The surface free energy $\gamma_S$ was calculated from Eq. (SI-1).

**Table 2**. Voltage rise and energy/cycle in samples SC-1 and SC-2.

**Table 3**. Characteristics of the CDLE cycle in samples SR-03, SR-23 and SR-51. Charging voltage 300 mV. $R_{discharge}$ = 110 Ω; switching time 1 min.

## FIGURE CAPTIONS

**Figure 1.** Schematic representation of the surface charge density in one of the electrodes vs. half the potential difference between them for two NaCl concentrations. The circuit assembly is represented for each branch. A possible CDLE cycle is represented by the points A,B,C,D; the blue-shadowed area measures the energy extracted.

**Figure 2.** Transmission electron microscope of the TE-11 activated carbon particles used. The bar size is 500 nm.

**Figure 3.** a) Picture of the electrodes; b) detail of the glass cell.

**Figure 4.** Example of one cycle through the four CDLE steps.

**Figure 5.** Model of the CDLE circuit.

**Figure 6**. Potential as a function of time of the CDLE cycle for different charging voltages in cells built with Norit films (a). Voltage rise (b) and transferred charge in step 3 (c) as a function of the charging voltage in the case of TE11 powder. The dashed lines are guides for the eye.

**Figure 7**. Specific pore size distribution for samples SC-1 and SC-2.

**Figure 8**.Voltage-time dependences during successive CDLE cycles for samples SC-1 and SC-2.

**Figure 9**. Pore size distributions of the carbon samples indicated.

**Figure 10**. Detail of the initial potential rise in CDLE cycles for samples SR-03, SR-23 and SR-51. The data have been shifted in time and voltage to make their origins coincident.

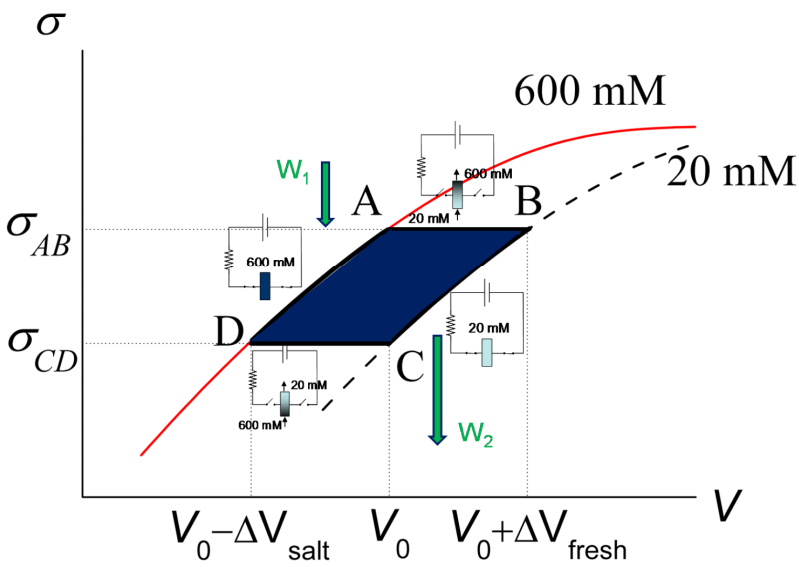


**Figure 1.** Schematic representation of the surface charge density in one of the electrodes vs. half the potential difference between them for two NaCl concentrations. The circuit assembly is represented for each branch. A possible CDLE cycle is represented by the points A,B,C,D; the blue-shadowed area measures the energy extracted.

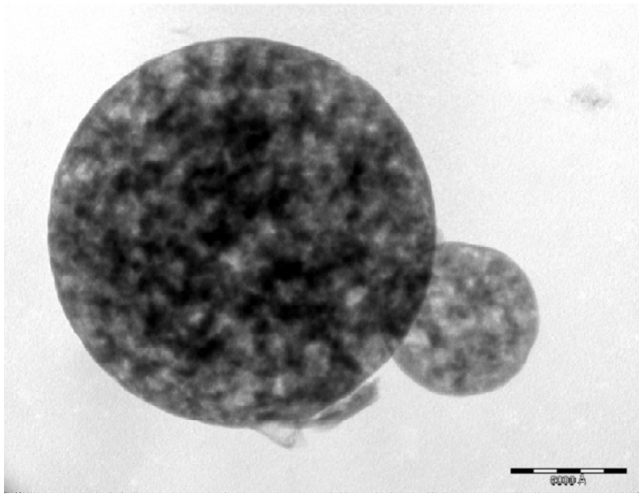

**Figure 2.** Transmission electron microscope of the TE-11 activated carbon particles used. The bar size is 500 nm.

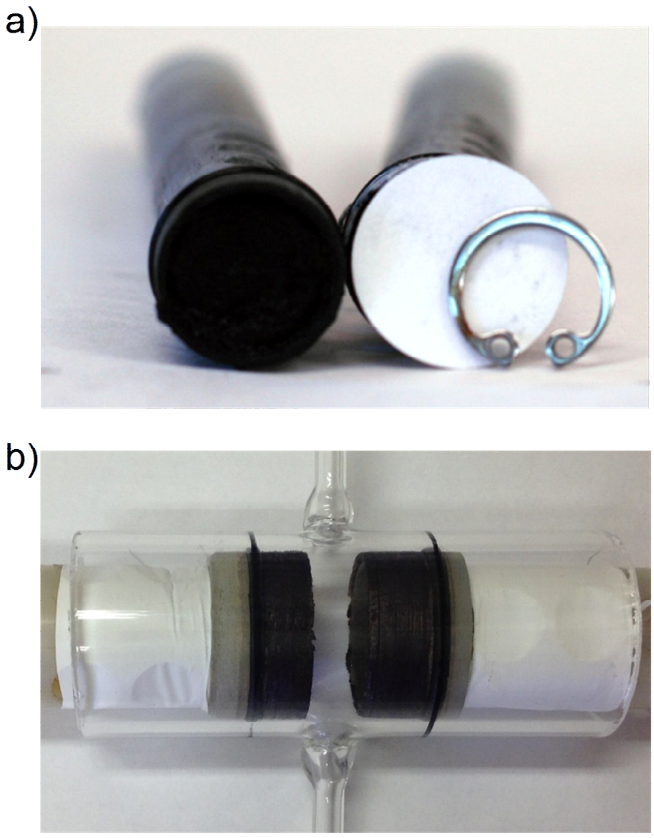


**Figure 3.** a) Picture of the electrodes; b) detail of the glass cell.

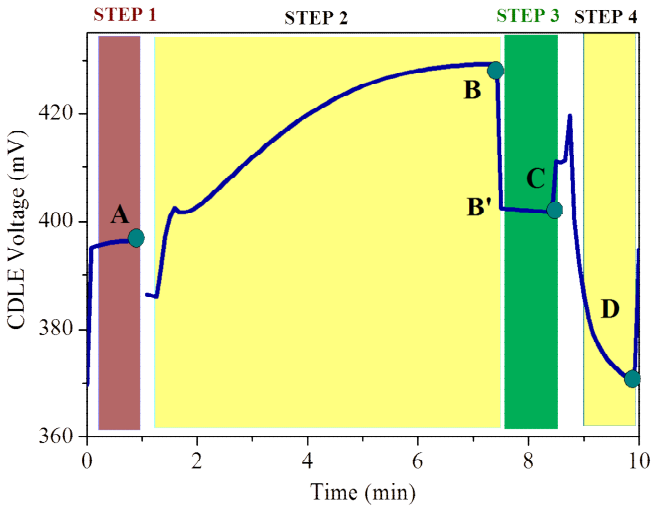


**Figure 4.** Example of one cycle through the four CDLE steps.

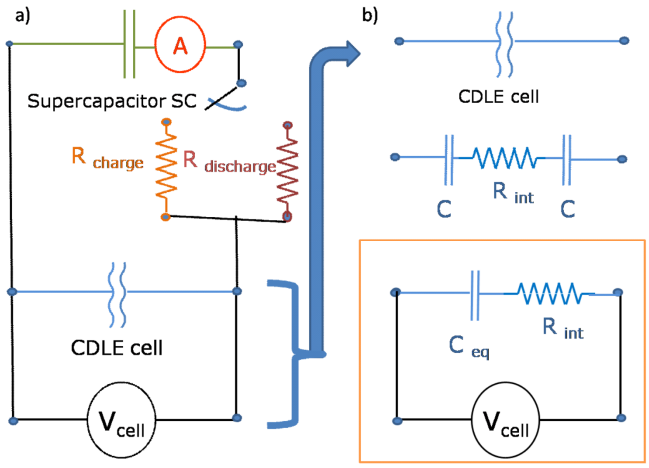


**Figure 5.** Model of the CDLE circuit.

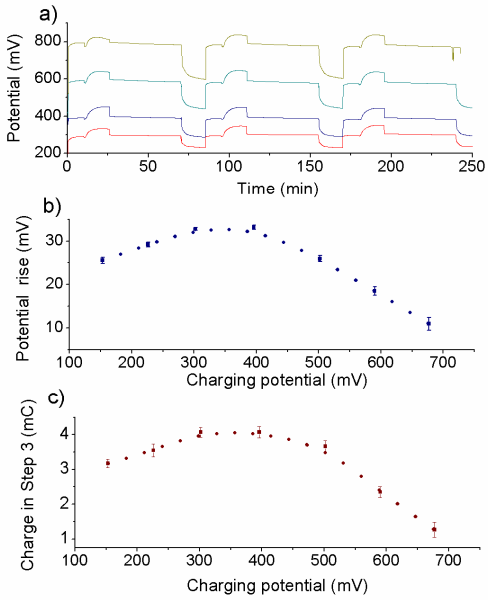


**Figure 6**. Potential as a function of time of the CDLE cycle for different charging voltages in cells built with Norit films (a). Voltage rise (b) and transferred charge in step 3 (c) as a function of the charging voltage in the case of TE11 powder. The dashed lines are guides for the eye.

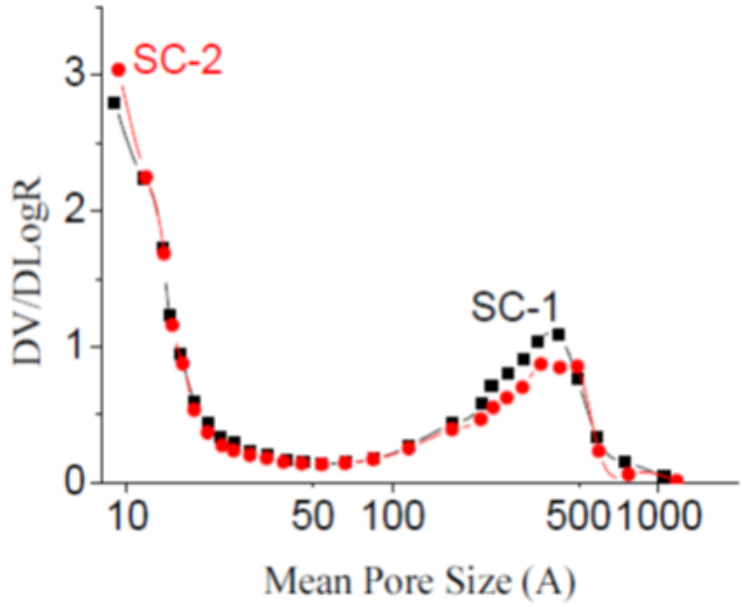


**Figure 7**. Specific pore size distribution for samples SC-1 and SC-2.

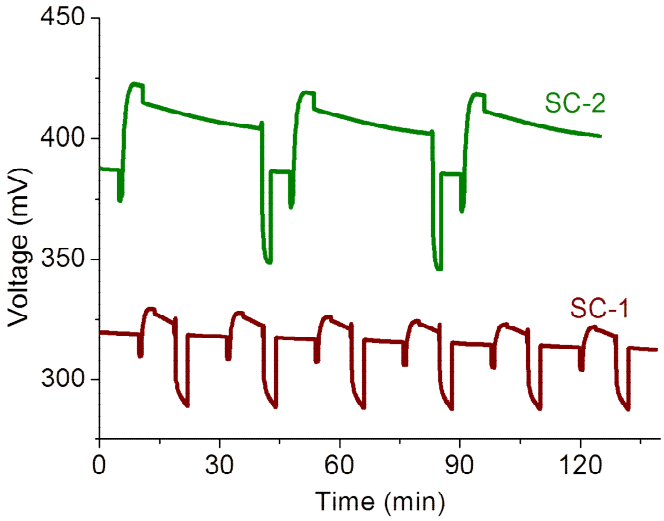


**Figure 8**.Voltage-time dependences during successive CDLE cycles for samples SC-1 and SC-2.

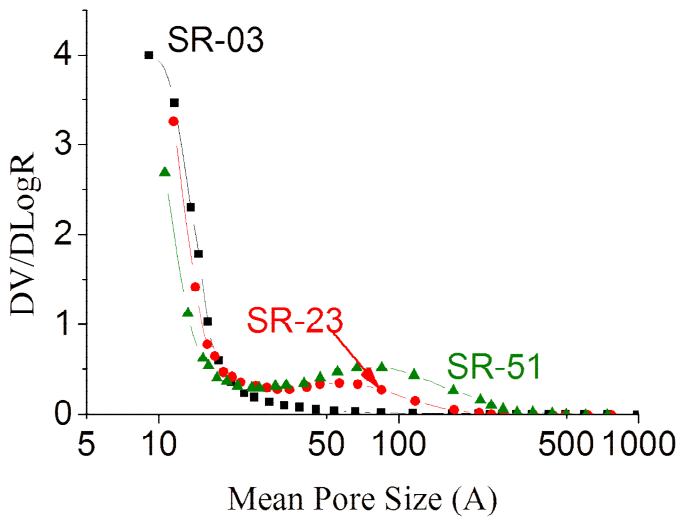


**Figure 9**. Pore size distributions of the carbon samples indicated.

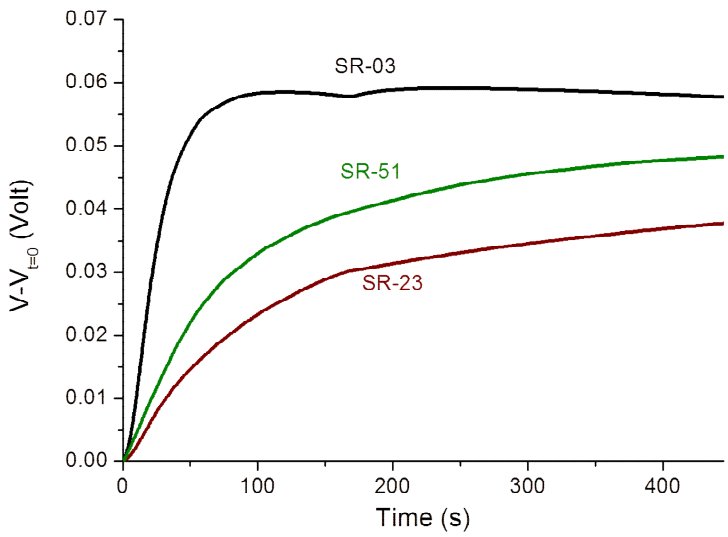


**Figure 10**. Detail of the initial potential rise in CDLE cycles for samples SR-03, SR-23 and SR-51. The data have been shifted in time and voltage to make their origins coincident.

**Table 1**. Advancing and receding contact angles of water on samples SC-1, SC-2, SR03, SR-23 and SR-51. The receding angle in SC-2 was not significantly distinct from zero. The surface free energy $\gamma_S$ was calculated from Eq. (SI-1).

| Sample | $\theta_a$ (°) | $\theta_r$ (°) | $\gamma_S$ (mJ/m$^2$) |
|---|---|---|---|
| SC-1 | 125 ± 3 | 84± 7 | 8.5± 1.6 |
| SC-2 | 29± 5 | -- | 66.0± 2.1 |
| SR-03 | 86± 5 | 49± 2 | 31 ± 4 |
| SR-23 | 110± 2 | 74± 8 | 16± 1 |
| SR-51 | 107± 3 | 61± 4 | 17± 2 |

**Table 2**. Voltage rise and energy/cycle in samples SC-1 and SC-2.

| Sample | Voltage rise (mV) | Energy/cycle (μJ) |
|---|---|---|
| SC-1 | 9.5 ± 0.7 | 6.7 ± 0.6 |
| SC-2 | 33.4 ± 0.9 | 680 ± 50 |

**Table 3**. Characteristics of the CDLE cycle in samples SR-03, SR-23 and SR-51. Charging voltage 300 mV. $R_{discharge}$ = 110 Ω; switching time 1 min.

| Sample | Voltage rise (mV) | $V_{AB'}$ (mV) | Transferred charge (mC) | Energy/cycle (μJ) |
|---|---|---|---|---|
| SR-03 | 52 ± 2 | 15 ± 1 | 5.7 ± 4 | 64 ± 7 |
| SR-23 | 30 ± 2 | 9 ± 1 | 3.0 ± 1 | 18 ± 3 |
| SR-51 | 48 ± 4 | 13 ± 1 | 3.4 ± 2 | 27 ± 3 |

# SUPPORTING INFORMATION

# Materials selection for optimum energy production by double layer expansion methods

*Guillermo R. Iglesias, María M. Fernández, Silvia Ahualli, María L. Jiménez, Oleksander P. Kozynchenko, Ángel V. Delgado*

## CARBON PREPARATION DETAILS

The sample hereafter denominated SC-1 was prepared by activation (40% burn-off) of mesoporous carbon beads (250-500 µm in diameter) derived from mesoporous phenolic resin beads prepared by the patented method of Tennison et al. [27]. The carbon sample SC-2 was prepared by oxidation of SC-1 in air at 320 $^{o}$C to give additional 15% burn-off and decorating the surface with oxygen containing functional groups [27]. SR-03 was prepared by straightforward activation at 900 $^{o}$C (50% burn-off) of microporous granular carbonisate of phenolic resin [27]. Activation of the same carbonisate with carbon dioxide at 800 $^{o}$C in the presence of catalytic quantities of calcium oxide resulted in preferential development of small mesopores to give samples SR-23 (35% burn-off) and SR-51 (44% burn-off). The synthesis of TE11 differed from the others in the fact that the starting resin was intensively stirred to create very fine resin beads, and ethylene glycol was added as pore former. The samples were then

vacuum-dried to remove this compound and activated to 35 % burn-off in $CO_2$. The specific surface areas of the carbons were ($m^2/g$): 1170 (TE11), 1423 (SC-1), 1489 (SC-2), 1870 (SR-03), 927 (SR-23) and 959 (SR-51). Finally, a commercially available sample (Norit DLC Super30, manufactured by Norit Nederland BV) was also employed in some experiments. The porous electrodes were formed either by packing the bare particles on the current collector or by previously forming layers deposited on a graphite film, as described in Liu et al. [9]. These carbon layers were made by mixing the activated carbon powder with a binder solution (polyvinylidene fluoride, PVDF in 1-methyl-2-pyrrolidinone, NMP).

## CIRCUIT MODELING

Experimental results are compared to circuit modelling. We show the cell current *I* and cell voltage *V* during the charging and discharging steps.

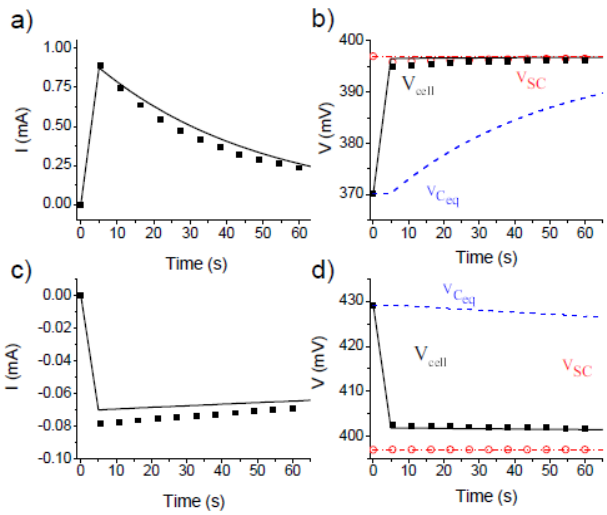


**Figure SI-1.** Model of the charge (a, b) and discharge (c, d) steps in the circuit shown in Figure 5. We assume $C_{eq}$ = 1.5 F, and the values used in the experiments: $R_{int}$ = 30 Ω for salt water and $R_{int}$ = 390 Ω for fresh water; $R_{charge}$ = 1 mΩ, $R_{discharge}$ = 70 Ω, $C_{SC}$ = 350 F. Full symbols:

experimental current and voltage data for the cell. Open symbols: potential of the external supercapacitor. Solid lines: predicted cell data. Dashed lines: calculated voltage of $C_{eq}$. Dash-dotted lines: prediction of the supercapacitor potential.

## EFFECTS OF INTERNAL AND LOAD RESISTANCES, AND OF SWITCHING TIMES

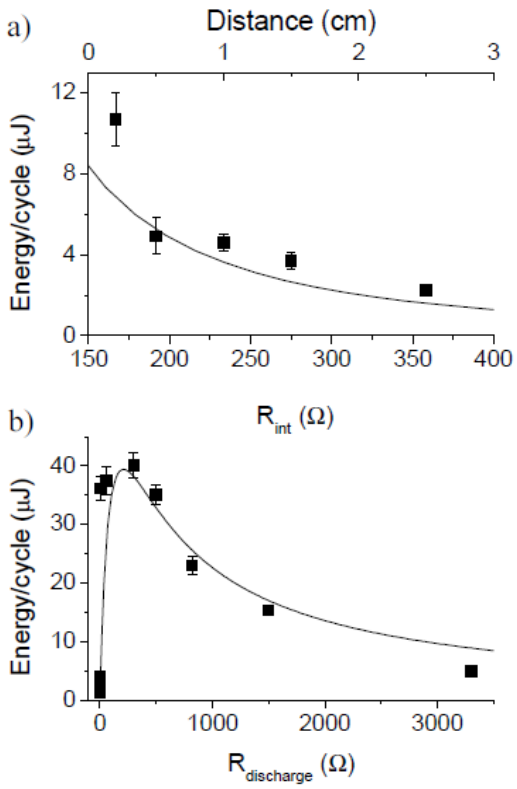


**Figure SI-2.** Extracted energy as a function of the distance between electrodes (a) and the external resistance in the discharging step (b). The lines indicate the equivalent circuit predictions for the following parameter choices: $C_{eq}$= 1.5 F, $C_{SC}$= 350 F. In (a) $R_{discharge}$= 3 Ω,

and $R_{int}$ in freshwater as indicated. In (b): $R_{int}$=200 Ω in freshwater, and $R_{discharge}$ as indicated. Sample TE11.

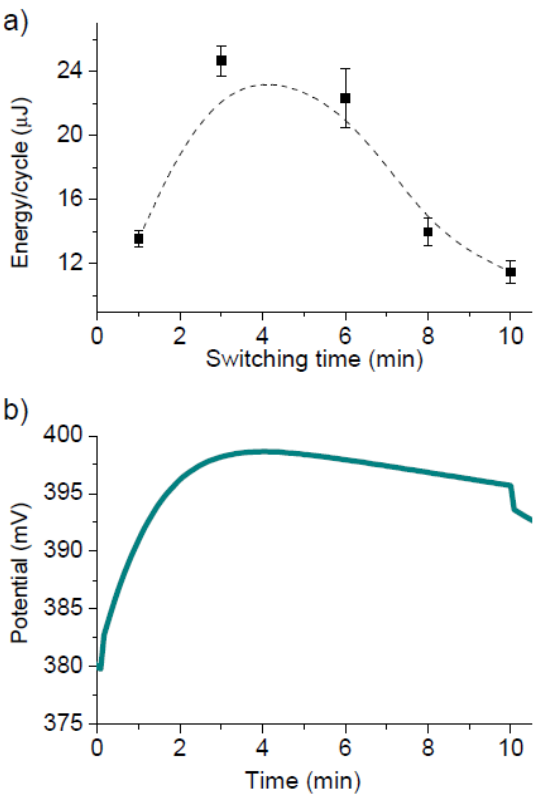


**Figure SI-3**. a) Extracted energy as a function of the rising time. The dotted line is a guide for the eye. b) Cell potential evolution during step 2. Sample: Norit film. $R_{discharge}$ = 330 Ω.

## SURFACE FREE ENERGY DETERMINATIONS

The *advancing contact angle* ($\theta_a$) is measured when a liquid droplet of known volume is carefully deposited on the solid surface. Once this angle is determined, the drop volume is reduced, thus retreating the contact line, and the *receding contact angle* ($\theta_r$) can be measured. It

is commonly assumed that during this process, a film of the liquid is left on the solid and thus the latter angle will be smaller than the former, because it is measured on an already wetted surface. The difference between the two angles is called *contact angle hysteresis* [31] and an approach has been proposed relating both angles to the surface free energy of the solid, $\gamma_S$, which is crucially important for our study [31, 32]. This can be done as follows:

$$\gamma_S = \frac{\gamma_L (1 + \cos\theta_a)^2}{2 + \cos\theta_a + \cos\theta_r} \qquad (1)$$

where $\gamma_L$ is the liquid surface tension, water in our case ($\gamma_L$ = 72.8 mN/m). The advancing contact angle was measured after depositing 6±2 µL droplets on the surface, and for the receding contact angle this volume was reduced to 4±2 µL.

One example is shown in Fig. SI-4.

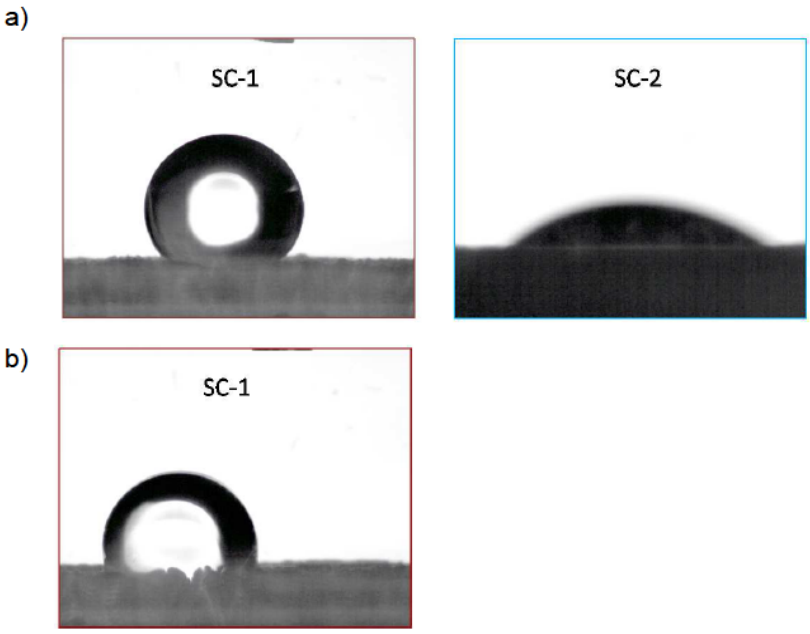

**Figure SI-4**. Droplets formed for advancing (a) and receding (b) contact angle measurements for carbons SC-1 and SC-2. The receding contact angle could only be measured for the former, and it was taken as zero for SC-2.

## SAMPLES WITH DIFFERENT PORE SIZES

Figure SI-5 gives information about the electrophoretic mobility in samples SR-03, SR-23 and SR-51. This quantity approximately proportional to the natural surface potential.

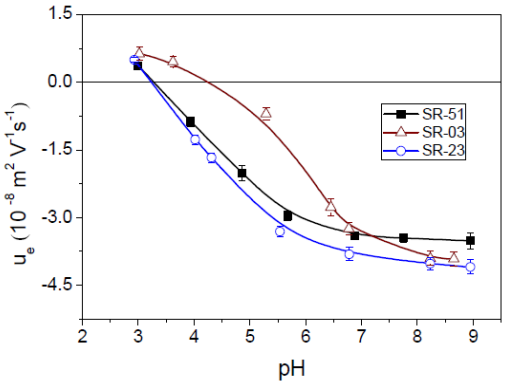


**Figure SI-5**. a) Electrophoretic mobility of particles of samples SR-03, SR-23 and SR-51 as a function of pH in 1 mM NaCl solution.

### ELECTROPHORETIC MOBILITY OF SC-1 AND SC-2

The electrophoretic mobility vs. pH is an indirect proof of increased hydrophilicity, considering that the presence of more dissociable groups per unit surface area will manifest in

both an increased hydrophilic character and an increased surface electric charge. Fig. SI-6 shows that the electrophoretic mobility of both samples is negative in most of the pH range, but only SC-1 presents an isoelectric point $pH_{iep}$ ~ 4, while SC-2 remains negative through the whole pH variation. This is a manifestation of a larger density of $OH^-$ ions, in the latter sample, after an oxidation treatment.

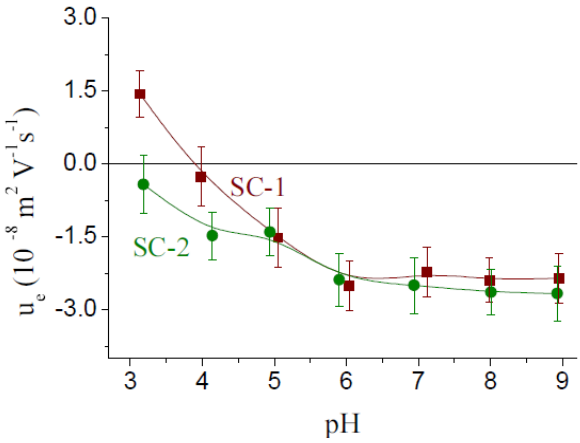


**Figure SI-6**. Electrophoretic mobility of the carbon particles SC-1 and SC-2 as a function of pH in a constant ionic strength of 1 mM NaCl.